THEORETICAL OVERVIEW OF JET PHOTOPRODUCTION AT HERA

MICHAEL KLASEN
Deutsches Elektronen-Synchrotron DESY, Theory Group,
Notkestrasse 85, D-22607 Hamburg, Germany
E-mail: michael.klasen@desy.de

ABSTRACT

We review the theoretical framework of jet photoproduction at HERA discussing the conceptual ideas, phenomenological models, and higher order perturbative calculations. Numerically, we study the physically interesting distribution of transverse energy within the observed jet, the real and virtual photon structure, and the proton structure at large x.

To appear in Proc. of "New Trends in HERA Physics", Ringberg, May 1997.

arXiv:hep-ph/9706292v2 14 Jul 1997

1. Theoretical Concepts

In electron-proton scattering at HERA the dominant fraction of the scattering events proceeds through photons with low virtuality Q^2.[a] Experimentally the electron is anti-tagged and remains in the beam-pipe. Theoretically the lepton tensor and phase space can then be factorized with the Weizsäcker-Williams approximation[1], which was improved recently through power-suppressed terms by Frixione et al.[2] The virtuality of the photon is less than 4 GeV^2, and it retains a fraction $y \in [0.2; 0.85]$ of the incident electron energy $E_e = 27.5$ GeV. The proton energy is 820 GeV.

Jet production in photon-proton collisions was first calculated in leading order (LO) of perturbative QCD by Owens[3]. The two-fold nature of direct and resolved processes and their separation on a kinematical basis were pointed out as a means to test the underlying partonic dynamics. It is thus possible to study the distribution of partons in the initial photon and proton and the spin of the exchanged particle.

Since then much effort has been spent on improving the tree-level understanding. Phenomenological models have been implemented into the Monte Carlo event generators PYTHIA[4], HERWIG[5], and PHOJET[6] employing parton showers, fragmentation models, and multiple interactions. Next-to-leading order (NLO) calculations for inclusive single-jet[7] and dijet production[8] provide perturbative correction factors, reduce the scheme and scale dependences, and allow for an implementation of jet definitions. Recently the first NLO analysis of the transition from real to virtual photoproduction of jets has been published[9].

Although several parametrizations exist for the parton distributions in the photon in NLO[10], the gluon is still poorly constrained by the data from $\gamma\gamma$ scattering at e^+e^- colliders and needs complementary measurements from γp. The situation is better for the parton densities in the proton[11], where photoproduction data might improve the data from deep inelastic and $p\overline{p}$ scattering at intermediate to large values of x. Except

[a] From 1994-1997, HERA operated with positrons instead of electrons. Since we will only be concerned with neutral current exchange, we use the term "electron" for positrons as well.

where indicated we use the GS96 and CTEQ4M parametrizations for the photon and proton, respectively.

2. Phenomenological Models

Perturbative QCD describes only the hard partonic scattering process and the scale evolution of the hadronic structure functions. The link between colored partons and real hadrons belongs to the non-perturbative domain and has to be fitted to data or guessed from phenomenological models. These models are implemented in Monte Carlo generators and compared in Table 1.

Table 1. Properties of different Monte Carlo generators.

Monte Carlo Generator	Parton Showers	Fragmen-tation	Multiple Interactions
PYTHIA	Initial+Final	String	Hard (optional)
HERWIG	Initial+Final	Cluster	Soft (optional)
PHOJET	Final	String	Soft and Hard

As a first step, one can attach additional angularly ordered partons to the hard process until the original parton reaches a maximum virtuality of $Q^2_{\max} < E^2_T$. In addition and deviating from the parton model, intrinsic transverse momenta are allowed for the partons in the hadrons up to $k_T < k_T^{\max}$ thereby introducing a second phenomenological parameter.

The second step consists in the fragmentation of the proliferated partons into hadrons. The Lund string model confines the color field between quarks into a color flux tube. The energy increases proportional to the distance between the quarks until the string breaks up and new quark-antiquark pairs are created. Hadrons are formed when the energy is too low for the string to break up according to a fragmentation function with two free parameters. Gluons appear as excitations and produce kinks in the string. Alternatively the cluster model starts with the splitting of gluons into $q\overline{q}$ pairs and the subsequent formation of color neutral clusters. Heavy clusters cascade into light clusters which then transform isotropically into hadrons.

Finally multiple interactions seem to be important at HERA to describe transverse energy flow and cross sections in the direction of the proton remnant at low E_T. They increase the multiplicity and energy flux and model interactions between the photon and the proton remnant. Secondary interactions are softer than the first scattering defined by E_T and can be of partonic or soft nature.

3. Next-to-Leading Order Calculations

The undesirable drawback of phenomenological models is the large number of free parameters that have to be tuned to data. These are not present in next-to-leading

order calculations where one calculates virtual corrections with internal particle loops and real corrections with soft and collinear radiation one order higher in the strong coupling constant α_s. The singularities can then be controlled through dimensional regularization and removed consistently through renormalization and factorization procedures. This avoids unphysical cut-off parameters, reduces the scheme and scale dependence, and allows for an implementation of jet definitions.

Real corrections are most easily calculated with the phase space slicing method. After approximation of the invariants and partial fractioning of the $2 \to 3$ matrix elements, we factorized the Born process and integrated the remaining singular kernels analytically up to an invariant mass cut-off $y_{\rm cut}$. Aurenche et al.[8] employed a transverse energy cut-off for the soft/collinear initial state, which does not appear in a related method for the single-jet case, and a cone cut-off for the collinear final state.[b] Harris and Owens integrated the soft and collinear regions separately[8]. The real emission outside the cut-offs is integrated numerically. This removes the dependence on the technical cut-off and introduces the experimental jet definition.

The subtraction method relies on a point-by-point subtraction of singularities in the numerical integration and has only been applied to the direct process by Bödeker[7]. The resolved process could, however, be adapted from an existing program in $p\overline{p}$ scattering[12].

4. Jet Definition Uncertainties

In hadronic collisions cluster algorithms of the JADE type combine particles not only into the hard jets but also into the remnant jets. This is avoided if a cone of size $R = 1$ in azimuth-rapidity space is used to define a jet. The Snowmass[13] accord determines the jet axis from the E_T weighted directions of all particles in the cone. Unfortunately it contains a number of ambiguities which render a matching between theory and experiment difficult[14].

Contrary to fixed cone algorithms, iterative cone algorithms can merge overlapping jets. This is not described by a NLO calculation with just three final state partons. If two partons have a distance between R and $2R$, they can be counted as one or two jets, and one has to avoid double-counting. The phenomenological parameter $R_{\rm sep}$ defining the distance of two partons can be used to model the narrower jets found by iterative cone algorithms.

In a recent study[15], we used this $R_{\rm sep}$ parameter to describe jet shapes $\rho(r)$ as measured by the ZEUS, CDF, and D0 collaborations. The result is compared to preliminary ZEUS data from 1994[16] which was obtained with an iterative cone algorithm and is shown in Figs. 1 and 2. It depends moderately on the rapidity η of the jet (Fig. 1) being broader in the forward direction and narrows slightly with the transverse energy E_T of the jet (Fig. 2). Whereas the curves with $R_{\rm sep} = 2$ correspond to

[b] See also the contribution by M. Fontannaz in these proceedings.

no $R_{\rm sep}$ and predict too broad jets, an average value of $R_{\rm sep} = 1.4$ describes the data rather well.

The uncertainties of the Snowmass cone definition are circumvented in the hadronic implementation of the k_T-cluster algorithm[17] with the same E_T-weighted recombination scheme as for Snowmass, but a different jet condition. One considers the distance of two particles in $\eta - \phi$ space. This corresponds to a unique value of $R_{\rm sep} = R$ in theory and experimentally assigns every hadron to a unique jet.

5. Real and Virtual Photon Structure

The determination of the structure of the photon is clearly one of the most important physics goals in photoproduction. Since the cross section drops rapidly with the transverse energy, most events at HERA have been observed at small E_T so far. They are dominantly produced by resolved photons and give access to the poorly constrained small-x region and the gluon density in the photon.

However at low E_T a separation of hard and soft physics is experimentally and theoretically difficult. Hadronization effects, jet definition uncertainties, energy pedestals around the jets, and multiple interactions between the remnant jets may play an important role. This can be seen in Figs. 3 and 4, where we compare our NLO calculation to preliminary 1994 data from ZEUS, again obtained with the iterative cone algorithm[18]. At $E_T > 14$ GeV, there is a clear excess of data over theory in the forward direction, which decreases continuously for larger E_T. We do not show a comparison with data obtained with a smaller cone size $R = 0.7$ which shows no excess in the forward region. Obviously the hard jets are better separated from the underlying event for smaller cones and there is no need for multiple interaction effects.

A second conclusion from Figs. 3 and 4 is that the jet definition uncertainty is of comparable size to the photon structure function uncertainty. Thus one either has to rely on the fitted value of $R_{\rm sep} = 1.4$ from jet shapes or use the k_T cluster algorithm.

In the backward region, where direct and quark initiated processes dominate, there is fairly good agreement with the data with a slight tendency of GRV to overestimate the measurement. This can be understood from the bigger quark contribution of GRV compared to GS96 at large values of x.

The kinematics of the partonic subprocess can be better constrained in dijet cross sections than in single cross sections, e.g. with the help of the variable $x_\gamma^{\rm OBS} = (E_{T_1} e^{-\eta_1} + E_{T_2} e^{-\eta_2})/(2yE_e)$. As long as one integrates over different bins, this variable is infrared-safe and there is no need to abandon it as put forward by Aurenche et al.[8] With the help of this variable, ZEUS separated direct and resolved regions experimentally and studied the dependence of the cross section on the average rapidity of the observed jets[19]. Unfortunately they constrained the E_T of both jets to the same minimal values. The theoretical predictions are then not infrared safe and depend on a phenomenological (Klasen and Kramer) or the technical cut-off (Harris

and Owens)[8]. This analysis employed the k_T cluster algorithm with $R = 1$ and exhibited again the excess of data over theory for the resolved dominated regions at low $x_\gamma^{\rm OBS}$ and E_T.

A new preliminary analysis of 1995 ZEUS data has been presented recently[20]. They measured the symmetrized dijet cross section $\mathrm{d}\sigma/\mathrm{d}E_T\mathrm{d}\eta_1\mathrm{d}\eta_2$ with the leading $E_T > 14$ GeV and $E_{T_2} > 11$ GeV in different rapidity bins and the full and upper region of $x_\gamma^{\rm OBS}$. The result is infrared safe and compared to our NLO predictions in Fig. 5 as a function of E_T and in Fig. 6 as a function of η_2. The general agreement is good for both GRV and GS96, even when both jets are in the forward region and the complete range in $x_\gamma^{\rm OBS}$ is covered. This may be due to the fairly large cuts on the E_T of both jets, which suppresses the underlying event. In the backward region, the calculation lies above the data and GS96 is slightly favored as was the case for the single-jet cross sections. In addition the systematic errors not shown here are quite prominent in the backward region. Since the data using the k_T algorithm were not yet available, we simulated the iterative cone algorithm with the optimized value of $R_{\rm sep} = 1.4$ for $R = 1$. This value should be lower in the backward region leading to a reduced theoretical prediction and better agreement with the data.

A new NLO program for virtual photoproduction[9] allows us to study the the transition to photons with virtuality P^2. Apart from using the unintegrated Weizsäcker-Williams approximation, the main difference consists in the analytic integration of the virtual photon initial state singularity. This singularity is then factorized and leads to a scheme- and P^2-dependent finite contribution which reduces to the real expression as $P^2 \to 0$. How this leading-logarithmic singularity compares to the two existing up-quark parametrizations in the virtual photon[21] is shown in Fig. 7. At low $P^2 = 1$ GeV^2 the evolution up to 50 GeV^2 produces many more up-quarks than just the single pair predicted perturbatively. At large $P^2 = 10$ GeV^2, GRS and SaS1M agree with the perturbative box-diagram[22].

ZEUS have also published P^2 dependent data on the ratio of resolved over direct contributions disentangled with the $x_\gamma^{\rm OBS}$ cut at 0.75[23]. As can be seen in Fig. 8 the NLO effects are large at $E_{T_1}, E_{T_2} > 4$ GeV. The lowest P^2 point for real photoproduction has much better statistics than the virtual photoproduction data and lies above the theory. This is to be expected since we are again in the soft region where remnant-remnant interactions are assumed to be important. At larger P^2, theory and data agree well in shape and normalization. We use the SaS1M LO parametrization, since NLO parton densities are not available in parametrized form and GRS does not contain charm.

6. Proton Structure at large x

The excess of high-Q^2 events in DIS at HERA have triggered a lot of speculation about new physics such as leptoquarks, R-parity violating supersymmetry, or contact

interactions. This kinematic regime can and should also be tested in photoproduction at large E_T, e.g. by measurements of $\mathrm{d}\sigma/\mathrm{d}E_T$, $\mathrm{d}\sigma/\mathrm{d}E_\gamma$, or $\mathrm{d}\sigma/\mathrm{d}M_{JJ}$. An unambiguous determination of new physics requires a precise knowledge of the Standard Model background. Due to phase space limitations, NLO corrections become increasingly important at the boundary of phase space at large E_T, whereas the uncertainty from the photon structure function becomes negligible. This can be extracted from Fig. 9, where the fractional contribution of direct photon-quark scattering accounts for more than 90% of the total single-jet cross section above $E_T = 100$ GeV. Therefore a precise knowledge of the quark distribution in the proton is required for $x > 0.4$.

In Fig. 10, we demonstrate the increase in the cross section that can be obtained with the larger quark densities of MRS(J') which were designed to describe the excess of CDF $p\overline{p}$ data at large E_T[24]. A factor of 1.5 seems possible here. Larger gluon distributions as proposed by CTEQ4(HJ)[11] only give a rise of 15%. It should be mentioned that MRS(J') fail to fit the low energy BCDMS data, whereas CTEQ4(HJ) are still consistent. Finally, a study of the scheme dependence might indicate further uncertainties here or in the gluon density.

7. Conclusions

A wealth of new and precise data coming from H1 and ZEUS in photoproduction has triggered increased theoretical interest. Three independent NLO calculations for real dijet production and the first NLO program for virtual photoproduction are now available. The interpretation of jets is improved with smaller cone sizes and the k_T cluster algorithm. This will allow for first stringent tests of the real photon parton density, especially of the gluon. More data and a parametrization of NLO parton densities are needed in virtual photoproduction. The access to large transverse momenta offers interesting studies of the proton structure at large x.

8. Acknowledgements

The author thanks the organizers of the Ringberg workshop for the kind invitation, G. Kramer and B. Pötter for their collaboration, and C. Glasman and Y. Yamazaki for making the preliminary ZEUS data available to him.

9. References

1. C.F.v. Weizsäcker, *Z. Phys.* **88** (1934) 612; E.J. Williams, *Phys. Rev.* **45** (1934) 729.
2. S. Frixione, M.L. Mangano, P. Nason, G. Ridolfi, *Phys. Lett.* **B319** (1993) 339.
3. J.F. Owens, *Phys. Rev.* **D21** (1980) 54.
4. T. Sjöstrand, hep-ph/9508391 (1995).

5. G. Marchesini et al., hep-ph/9607393 (1996).
6. R. Engel, *Z. Phys.* **C66** (1995) 203.
7. H. Baer, J. Ohnemus, J.F. Owens, *Phys. Rev.* **D40** (1989) 2844; L.E. Gordon, J.K. Storrow, *Phys. Lett.* **B291** (1992) 320; P. Aurenche, M. Fontannaz, J.P. Guillet, *Phys. Lett.* **B338** (1994) 98; D. Bödeker, G. Kramer, S.G. Salesch, *Z. Phys.* **C63** (1994) 471; M. Klasen, G. Kramer, S.G. Salesch, *Z. Phys.* **C68** (1995) 113.
8. M. Klasen, G. Kramer, *Z. Phys.* **C72** (1996) 107, hep-ph/9611450 (1996); P. Aurenche, L. Bourhis, M. Fontannaz, J.P. Guillet *Proc. of "Future Physics at HERA"*, Hamburg (1996) 570; B.W. Harris, J.F. Owens, hep-ph/9704324 (1997).
9. M. Klasen, G. Kramer, B. Pötter, hep-ph/9703302 (1997).
10. M. Glück, E. Reya, A. Vogt, *Phys. Rev.* **D45** (1992) 3986; L.E. Gordon, J.K. Storrow, *Phys. Lett.* **B291** (1992) 320, *Nucl. Phys.* **B489** (1997) 405; P. Aurenche, M. Fontannaz, J.P. Guillet, *Z. Phys.* **C64** (1994) 621.
11. A.D. Martin, R.G. Roberts, W.J. Stirling, *Phys. Lett.* **B387** (1996) 419; H.L. Lai et al., CTEQ Collaboration, *Phys. Rev.* **D55** (1997) 1280.
12. S.D. Ellis, Z. Kunszt, D.E. Soper, *Phys. Rev. Lett.* **64** (1990) 2121.
13. J.E. Huth et al., *Proc. of the 1990 DPF Summer Study on High Energy Physics*, Snowmass CO (1992) 134.
14. J. Butterworth, L. Feld, M. Klasen, G. Kramer, *Proc. of "Future Physics at HERA"*, Hamburg (1996) 554.
15. M. Klasen, G. Kramer, hep-ph/9701247 (1997).
16. M. Derrick et al., ZEUS Collaboration, Contribution to the XXVIII. ICHEP, Warsaw (1996) pa 02-043.
17. S.D. Ellis, D.E. Soper, *Phys. Rev.* **D48** (1993) 3160.
18. M. Derrick et al., ZEUS Collaboration, Contribution to the XXVIII. ICHEP, Warsaw (1996) pa 02-041.
19. M. Derrick et al., ZEUS Collaboration, Contribution to the XXVIII. ICHEP, Warsaw (1996).
20. M. Derrick et al., ZEUS Collaboration, Contribution to PHOTON 97, Egmond aan Zee (1997).
21. M. Glück, E. Reya, M. Stratmann, *Phys. Rev.* **D51** (1995) 3220; G.A. Schuler, T. Sjöstrand, *Phys. Lett.* **B376** (1996) 193.
22. B. Pötter, Ph.D. Thesis, Universität Hamburg (1997), DESY 97-138, hep-ph/9707319.
23. M.L. Utley, ZEUS collaboration, *Proc. of "HEP95"*, Brussels (1995) 570; C. Foudas, ZEUS collaboration, *Proc. of "DIS96"*, Rome (1996) 275.
24. E.W.N. Glover, A.D. Martin, R.G. Roberts, W.J. Stirling, *Phys. Lett.* **B381** (1996) 353.

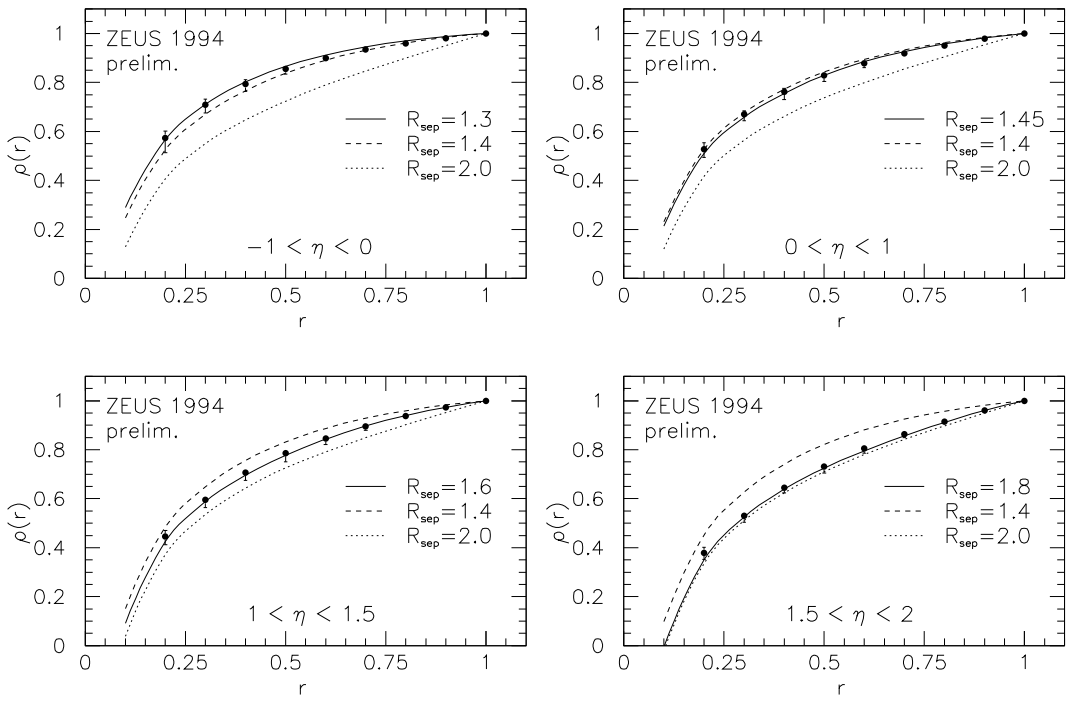

Fig. 1. *Jet shape $\rho(r)$ for single-jet photoproduction integrated over $E_T > 14$ GeV and four different regions of η. We compare our results using the Snowmass convention with $R = 1$ and three different values of $R_{\rm sep}$ to preliminary 1994 data from ZEUS.*

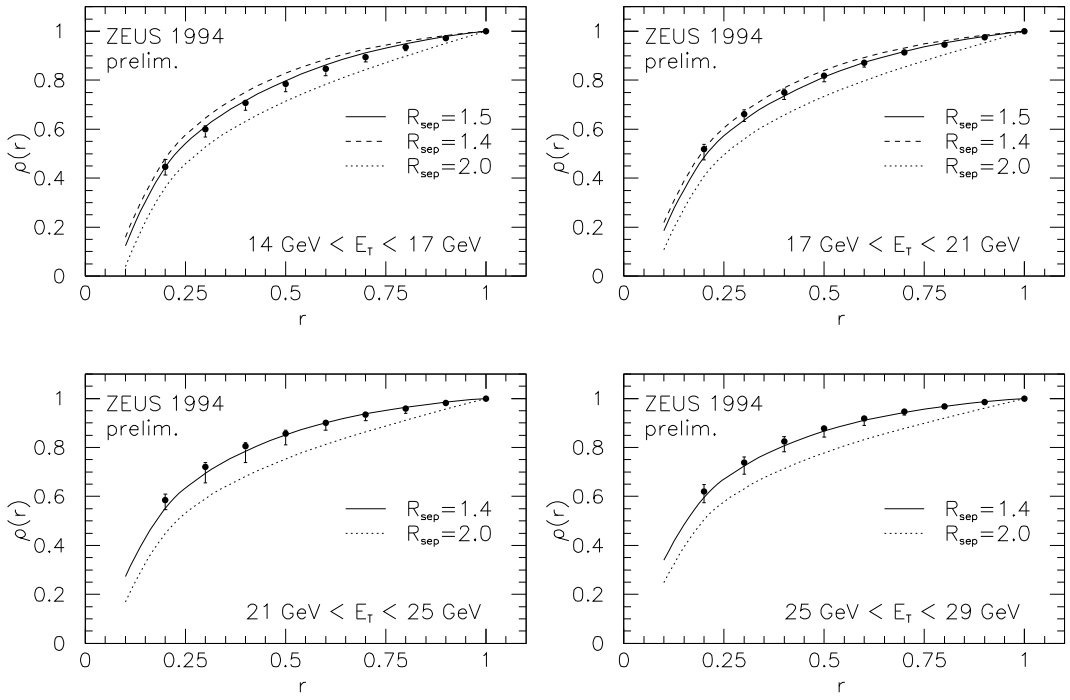

Fig. 2. *Jet shape $\rho(r)$ for single-jet photoproduction integrated over $-1 < \eta < 2$ and four different regions of E_T. We compare our results using the Snowmass convention with $R = 1$ and different values of $R_{\rm sep}$ to preliminary 1994 data from ZEUS.*

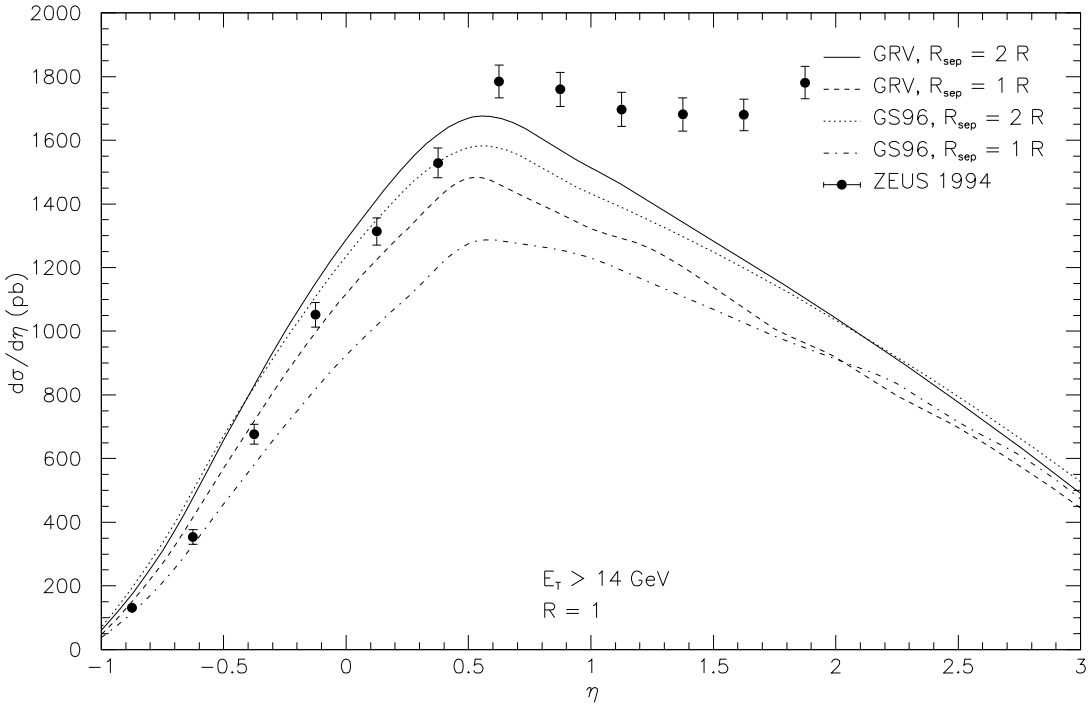

Fig. 3. *Rapidity dependence of the single-jet photoproduction cross section integrated above $E_T > 14$ GeV. We compare our NLO prediction with GRV and GS96 photon parton densities and the two extreme values of $R_{\rm sep} = 1R, 2R$ to preliminary 1994 data from ZEUS.*

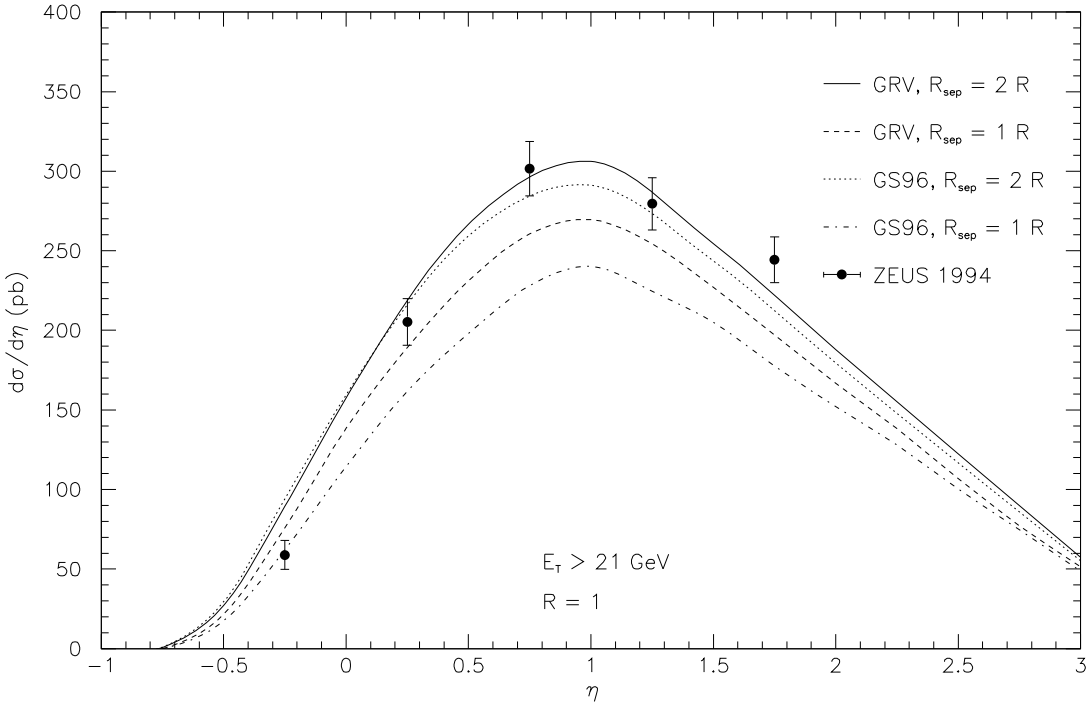

Fig. 4. *Same as Fig. 3 for $E_T > 21$ GeV.*

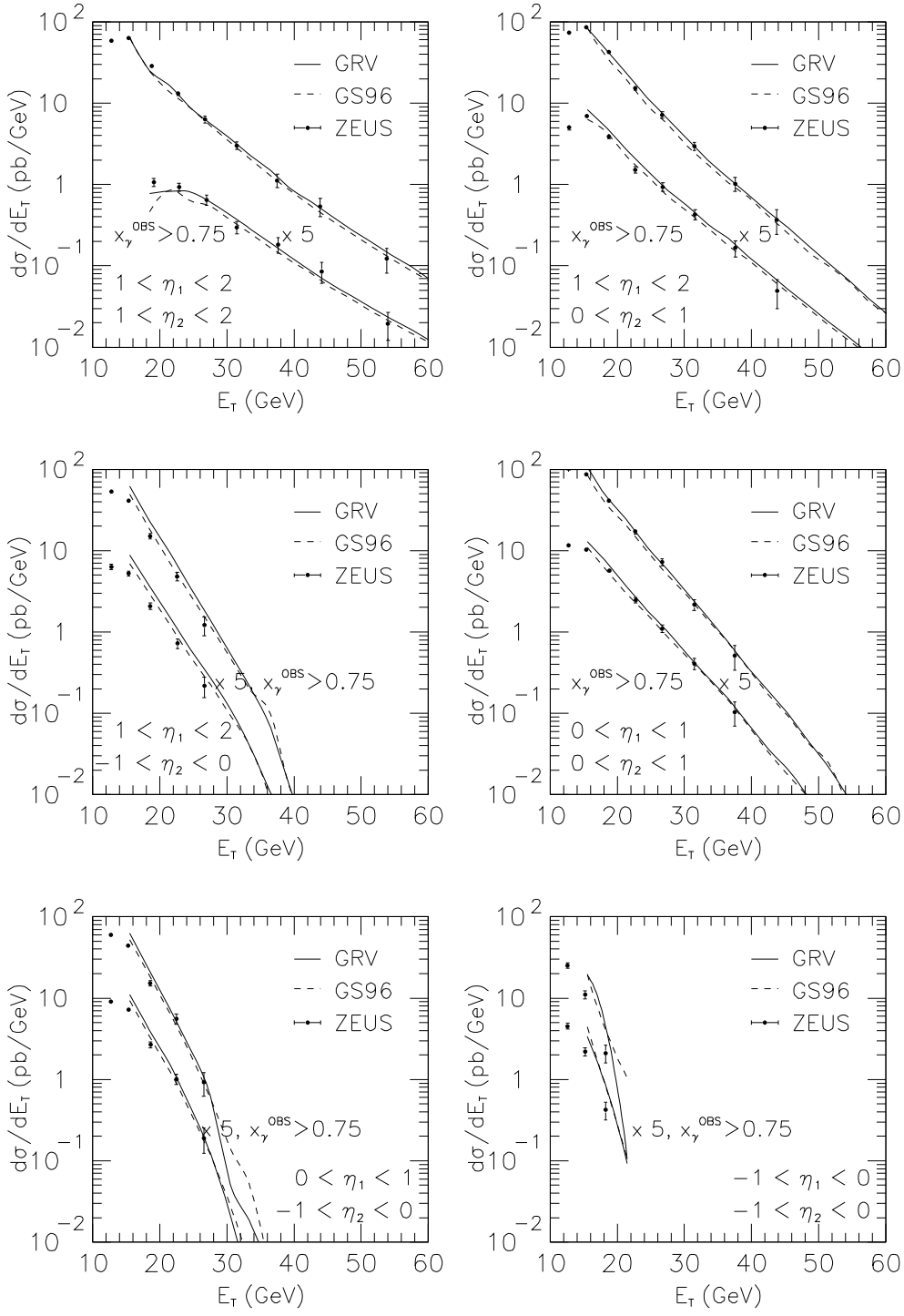

Fig. 5. *E_T dependence of the symmetrized dijet photoproduction cross section integrated over different rapidity bins. We compare our NLO prediction with GRV and GS96 photon parton densities and the full and upper range of $x_\gamma^{\rm OBS}$ to preliminary 1995 data from ZEUS.*

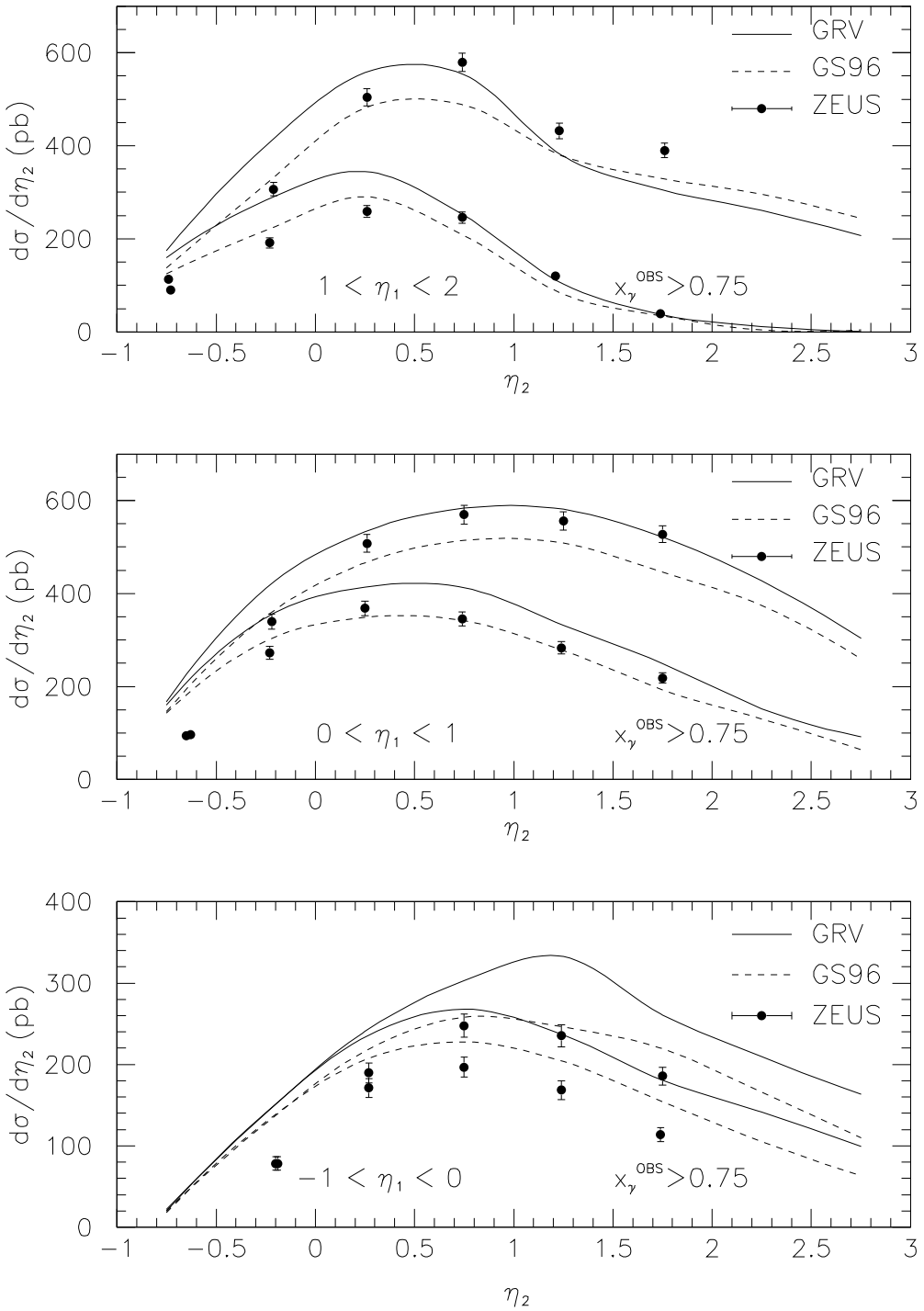

Fig. 6. *η_2 dependence of the symmetrized dijet photoproduction cross section integrated over $E_T > 14$ GeV and $E_{T_2} > 11$ GeV. We compare our NLO prediction with GRV and GS96 photon parton densities and the full and upper range of $x_\gamma^{\rm OBS}$ to preliminary 1995 data from ZEUS.*

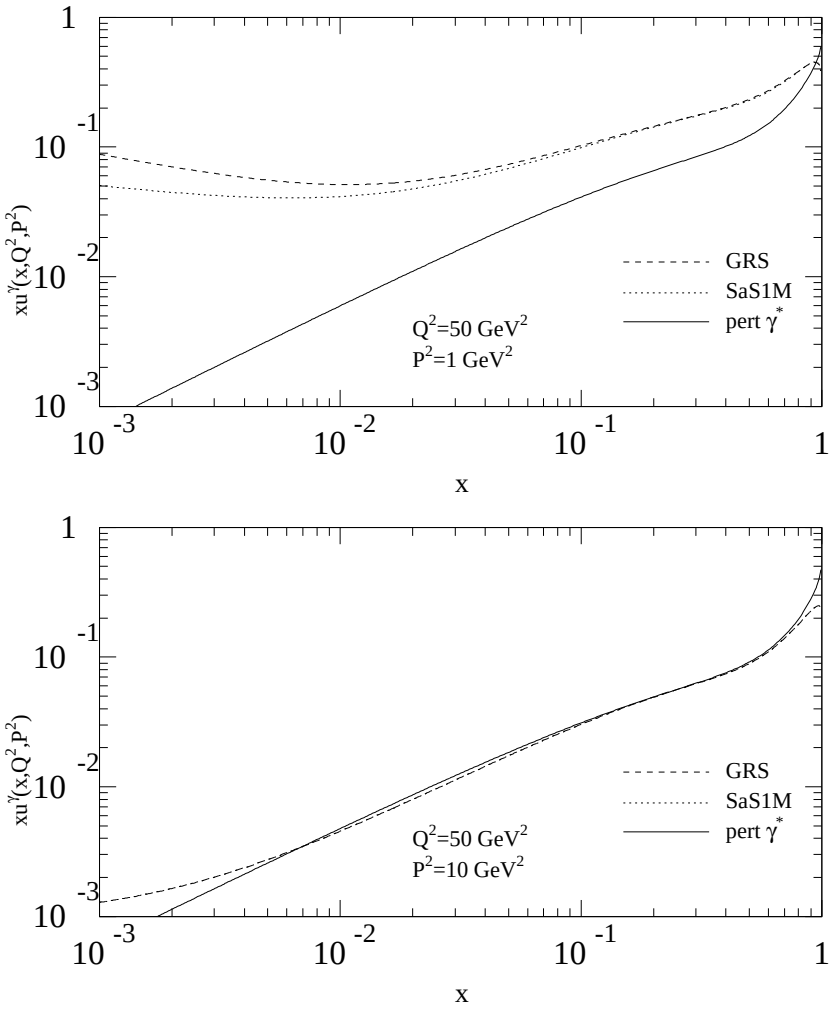

Fig. 7. *Up-quark distributions in the virtual photon as function of x. We compare the GRS and SaS1M parametrizations with the perturbative result for $P^2 = 1$ and 10 GeV^2* [22].

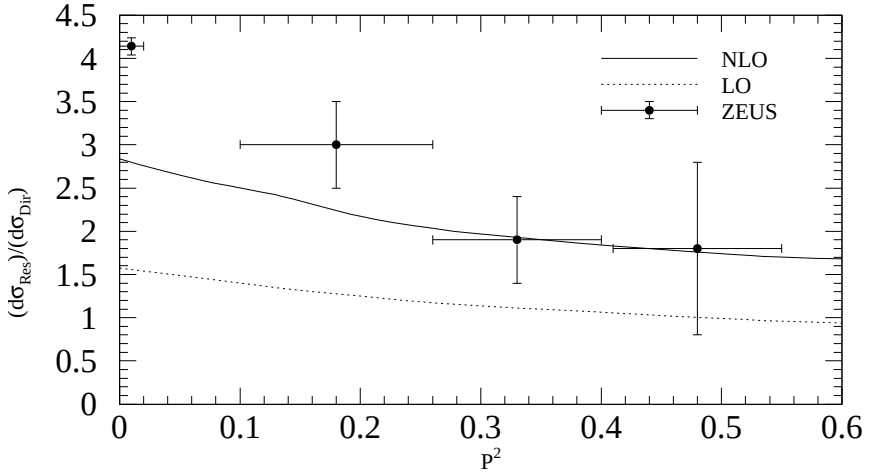

Fig. 8. *Ratio of resolved over direct contributions defined with the $x_\gamma^{\rm OBS}$ cut at 0.75 for $E_{T_1}, E_{T_2} > 4$ GeV using the SaS1M virtual photon structure with four flavors.*

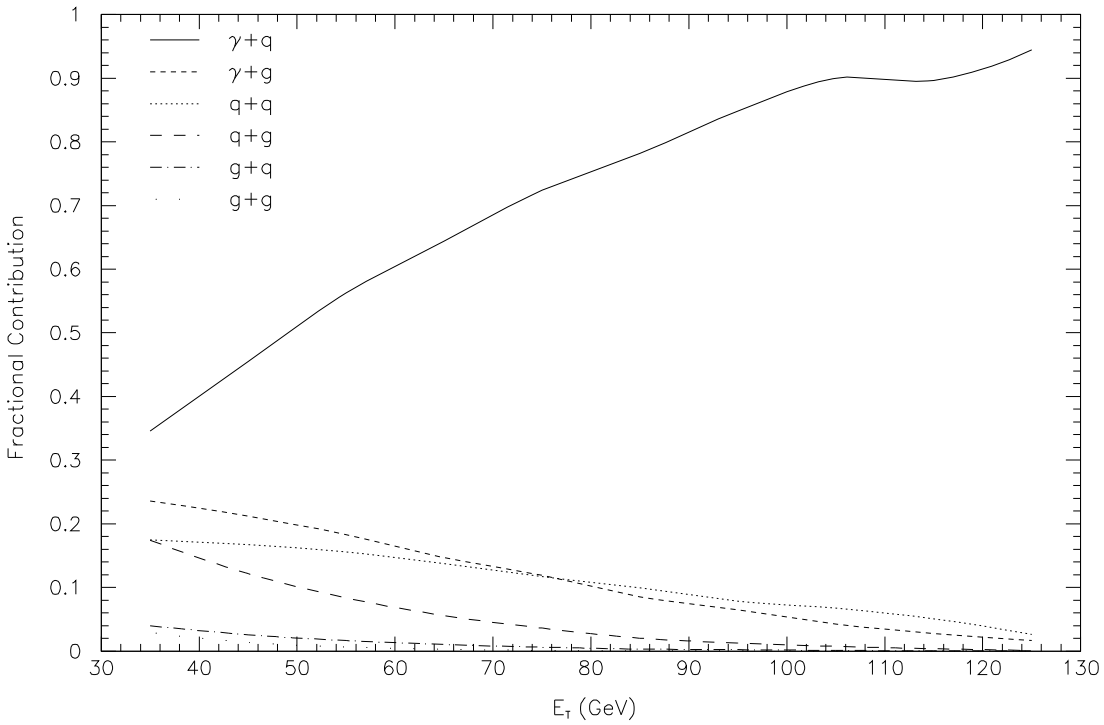

Fig. 9. *Fractional Contribution of direct and resolved partonic subprocesses as function of E_T in the single-jet photoproduction cross section.*

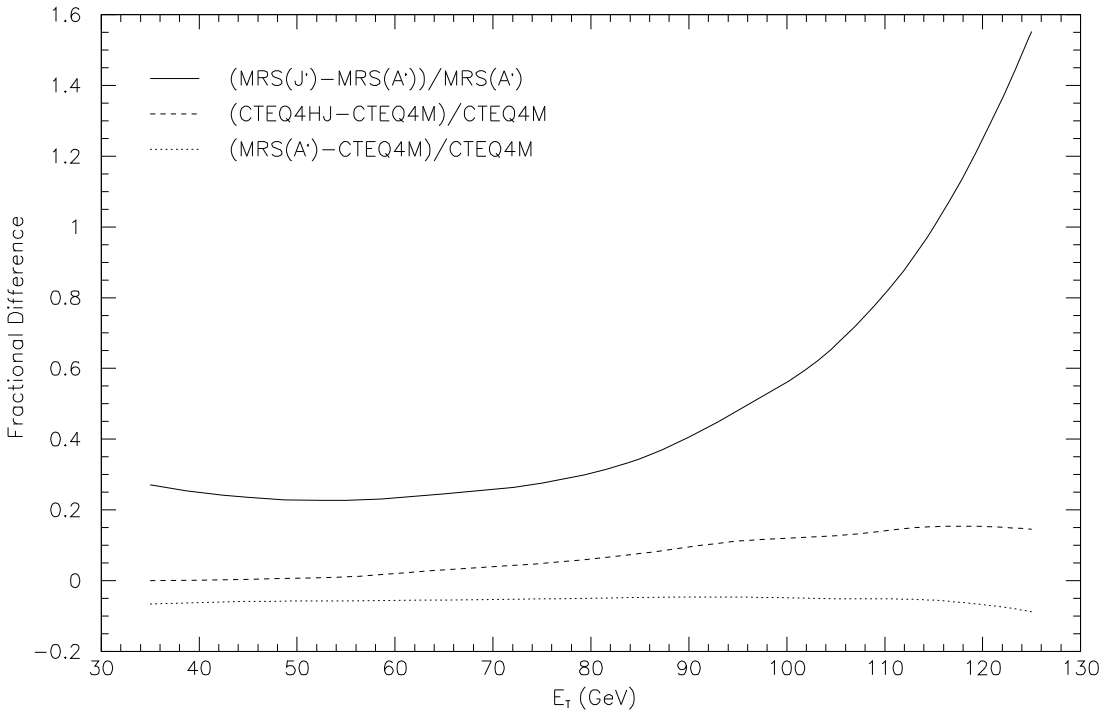

Fig. 10. *Fractional difference of different proton structure functions as function of E_T in single-jet photoproduction compared to standard parametrizations.*